

Feeding the black hole with condensing accretion flows: radiatively efficient and radiatively inefficient cases.

Sergei Nayakshin

Max-Planck-Institut für Astrophysik, Karl-Schwarzschild-Str. 1, 85740 Garching, Germany

2003 Xxxxx XX

ABSTRACT

We study the accretion flow of a hot gas captured by the black hole gravity in the presence of a thin cold accretion disk. Such geometrical arrangement is expected in Active Galactic Nuclei (AGN) and in galactic X-ray binary systems because both hot and cold gases are present in the black hole vicinity. Previous astrophysical literature concentrated on the evaporation of the cold disk in the classical heat conduction limit. Here we consider the inverse process, i.e. condensation of the hot gas onto the cold disk. We find two distinct condensation regimes. (i) In the classical thermal conduction limit, the radiative cooling in the hot gas itself force condensation above a certain critical accretion rate. Most of the flow energy in this case is re-emitted as X-ray radiation. (ii) Below a certain minimum accretion rate, the hot electrons are collisionless and the classical heat flux description becomes invalid. We use the “non-local” heat flux approach borrowed from the terrestrial laser heated plasma experiments. Due to their very large mean free path, the hot particles penetrate deep into the cold disk where the radiative losses are significant enough to enable condensation. In this case the hot flow energy is inconspicuously re-radiated by the transition layer in many UV and especially optical recombination lines (e.g., $Ly\alpha$, $H\alpha$, $H\beta$) as well as via the optically thick disk emission. We derive an approximate analytical solution for the dynamics of the hot condensing flow. If the cold disk is inactive, i.e. accumulating mass for a future accretion outburst, then the two-phase flows appear radiatively inefficient. These condensing solutions may be relevant to Sgr A*, low luminosity AGN, and transient binary accreting systems in quiescence.

1 INTRODUCTION

An optically thick accretion disk (e.g., Shakura & Sunyaev 1973) appears to be an important part of the accretion flow of gas into the black hole (BH) or a compact object. This conclusion is supported by spectral energy distributions (SED; see Elvis et al. 1994; Ho 1999; and Fig. 1 in Gierlinski et al. 1999), double peaked emission line profiles (e.g. McClintock et al. 2003; and references in Ho 2003), and eclipse mapping of binary systems (e.g. Wood et al. 1986). Even for Sgr A*, a very dim source, there is now a suspicion that a cold *inactive*, i.e. not accreting, disk may be present (Nayakshin, Cuadra & Sunyaev 2004).

There is also a significant amount of hot ($T > 10^7$ K) gas at large distances from the BH in galactic nuclei. In the best studied cases this hot gas is observed as close as its capture radius (e.g. in the giant elliptical galaxy and a LLAGN M87 [Di Matteo et al. 2003]; and in Sgr A* [Baganoff et al. 2003]), meaning that accretion of this hot gas on the BH is unavoidable. In galactic binary systems, a diffuse hot gas may be present near the disk outer rim due to a shock in the hot spot, if the radiative cooling time is longer than dynamical time. A shocked captured stellar wind from the secondary is another source of hot gas (and it may also form the cold disk itself; Kolykhalov & Sunyaev 1980).

Thus the accretion flow at large distances is often a two-flow problem (see Figure 1). Thermal conduction in a multi-phase medium leads to either evaporation of the cold gas, or vice versa, condensation of the hot gas (e.g., Zel’dovich & Pickel’ner 1969; Penston & Brown 1970). In reference to accretion flows, Meyer & Meyer-Hofmeister (1994; MMH94 hereafter) were the first to study the mass exchange between the cold disk and the corona. Their pioneering study, extended later by, e.g., Liu, Meyer & Meyer-Hofmeister (1997); Dullemond (1999); Rózańska & Czerny (2000a,b), showed that the cold disk evaporates at low coronal accretion rates. At large accretion rates the radiative cooling suppresses the corona (Rózańska & Czerny 2000a). The magnitude of the viscosity coefficient, α (Shakura & Sunyaev 1973), was shown to be extremely important. In all the models the evaporation rate decreases very strongly with decreasing α (e.g. Meyer-Hofmeister & Meyer 2001). Recently, Liu, Meyer & Meyer-Hofmeister (2004) found condensing solutions for a sufficiently small value of the viscosity parameter.

Here we aim to study the condensation process systematically, i.e. attempting to cover a broad range of accretion rates in the hot flow. We first review the classical thermal conduction case. As expected, we recover qualitatively the results previously obtained by the above referenced authors.

arXiv:astro-ph/0402469v1 19 Feb 2004

Namely, when the heat flux is classical, we find condensation at high and evaporation at low coronal accretion rates (§2). The critical accretion rate (at which no mass exchange between the disk and the hot corona takes place) is a strong function of α (§§2.2 & 6).

We then point out that for every value of α , there exists an accretion rate below which the classical thermal conduction treatment becomes invalid since the hot electron mean free path, λ , is long compared with the flow height scale, H . To study the problem in this limit, we use a modified (see §§ 2.1 & 3) prescription for the heat flux that is borrowed from the laser-heated plasma experiments. The heat flux is then proportional to the saturated heat flux coefficient, $\phi \leq 1$. While this case still requires a future physical kinetics treatment, we show that there may exist an additional condensation regime. In this regime the hot particles penetrate deep into the cold gas. The cold gas density turns out to be great enough to re-radiate the deposited energy away, enabling condensation. With the help of certain approximations, we build an analytical solution (§§ 4 & 5) for the radial structure of the hot flow in this case.

We put our results into the context of the previous work in §6, where we determine the type of solution for a given combination of parameters (accretion rate, radius, α and ϕ). We discuss the expected spectra from the two types of the condensing flows in §7. The classical thermal conduction condensing flow emits mainly in X-rays. Such solutions apply at relatively high accretion rates, and therefore they are likely to be relevant to bright or medium-bright AGN, such as Seyfert Galaxies. Due to these high accretion/condensation rates, the cool disk is probably active, meaning that the SED of these sources would be dominated by the emission from the small scale accretion disk in the vicinity of the last stable orbit. Such flows would obviously be radiatively efficient.

The second (non-local) condensation regime is applicable at lower accretion rates. It is therefore possible that accretion disks fed by condensation at these low rates would be inactive, as in quiescent states of transient binary sources. In this case the hot gas, settling onto the cold disk, effectively stops accreting. The hot accretion flow is thus terminated at some large distance away from the central object, which implies that the radiation emitted by such a flow will be much less luminous than expected from a flow onto the black hole. Furthermore, these flows may be quite dim in X-rays since the radiative cooling in the corona itself is small. The cold disk serves as a huge cooling plate (radiator) for the hot flow. The SED of such flows would then be dominated by their infra-red/optical thermal-like bumps rather than UV or X-ray frequency regions. We suggest that this radiative “inefficiency” (rather a time-delayed accretion) of condensing flows may be one of the reason why some LLAGN, and the galactic black hole Sgr A*, appear underluminous.

2 CLASSICAL THERMAL CONDUCTION IN TWO-PHASE FLOWS

2.1 Basic physics of thermal conduction

Figure 1 shows a sketch of geometry that we envisage in this paper. The hot flow is sandwiching a very cold and thin disk located in the midplane. A thin (compared with R)

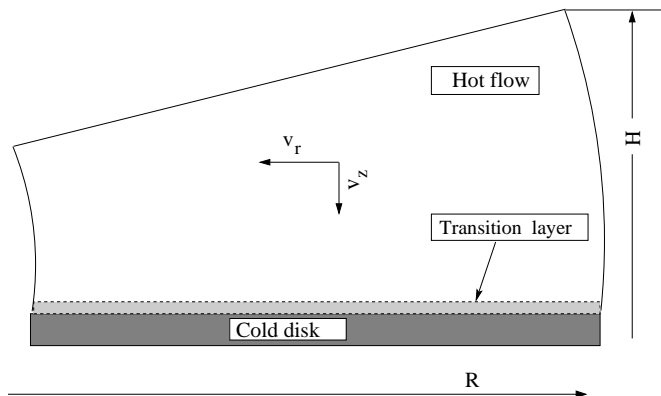


Figure 1. Geometry of the problem (shown for $z > 0$ only). The hot flow (corona) sandwiches a cold accretion disk. A transition layer heated by hot coronal electrons (§3) develops on the top of the cold disk. In the limit of collisionless thermal conduction, both the transition layer and the disk are thick to coronal electrons, and are very geometrically thin. In contrast, the corona is thin to coronal electrons (since $H \lesssim \lambda$), but is geometrically thick. Depending on conditions, the hot flow may be condensing (positive v_z) or evaporating. In the classical thermal conduction limit, the transition layer becomes optically thick to hot electrons. The layer’s geometrical thickness also increases.

transition layer develops between the corona¹ and the disk. Since the cold disk viscous time is very long, the disk can be treated as stationary.

The physics of the mass exchange between the two flows depends greatly on the heat flow from the hot to the cold gas. When collisions are abundant, i.e the mean free path for electron energy exchange, λ , is smaller than the temperature scale height, $L_T = T/|\nabla T|$, the classical (Spitzer & Harm 1953; Spitzer 1962) heat conductivity is used. The thermal heat flux, F , in this case is given by

$$\vec{F} = \vec{F}_{cl} = -k(T)\nabla T, \quad (1)$$

where T is the temperature (we will assume that electron temperature is equal to the proton’s temperature), $k(T)$ is the conductivity coefficient given by

$$k(T) = 1.84 \times 10^{-5} T^{5/2} / \ln \Lambda_c \text{ erg cm}^{-1} \text{ s}^{-1} \text{ K}^{-1}, \quad (2)$$

where $\ln \Lambda_c \sim 30$ is the Coulomb logarithm. The heating or cooling rate due to thermal conduction is

$$H_{cl} = -\text{div } \vec{F}. \quad (3)$$

For reference,

$$\lambda \simeq 10^4 T^2 / n \text{ cm} \quad (4)$$

(Spitzer 1962), where n is the gas density in cm^{-3} . If collisions are rare, i.e. $\lambda > L_T$, the classical formula overestimates the heat flux. The electron conduction is then artificially limited to (e.g. Parker 1963; Cowie & McKee 1977) the saturated heat flux:

$$F_{\text{sat}} = 5\phi\rho c_s^3, \quad (5)$$

¹ Throughout the paper, we shall use the terms “corona” and the “hot flow” interchangeably, although we do not assume that the origin of the corona is the cold disk.

where P and ρ are the gas pressure and density, respectively, $c_s^2 = P/\rho$ is the local isothermal sound speed of the gas, and $\phi \leq 1$ is the saturation coefficient. Even though magnetic fields may be important in reducing the thermal conductivity (see Appendix), in what follows their effects are included only through the magnitude of ϕ . A more detailed discussion of thermal conductivity in the saturated regime is given in §3.

2.2 Classical evaporation or condensation

Numerically accurate global evaporating solutions were obtained by MMH94, and that for condensation by Rózańska & Czerny (2000a). Here we only wish to establish the sign of the mass exchange between the two flows for given *local* conditions in the hot gas. For the sake of simplicity and generality, we approximate the geometry (Fig. 1) as planar, and neglect possible winds. In this setup the problem is similar to that of an infinite plane-parallel two-phase system studied by Zel'dovich & Pikel'ner (1969), and Penston & Brown (1970). In such a system, for a subsonic flow, the entropy equation (for adiabatic index $\gamma = 5/3$ and for $v_z > 0$ for downward direction; Fig. 1) is

$$-\rho v_z \frac{5k_B}{2\mu} \frac{dT}{dz} + \frac{dF}{dz} = q_+ - \Lambda(T)n^2, \quad (6)$$

where z is the vertical coordinate, q_+ is the heating rate in $\text{erg}/\text{cm}^3/\text{sec}$, $\Lambda(T)$ is the usual optically thin cooling function, and k_B and μ are the Boltzmann's constant and the mean molecular weight in the corona. Note that the subsonic flow assumption can be verified a posteriori: as results of Cowie & McKee (1977) for evaporation of spherical clouds show, the flow is always subsonic when the heat flux is classical. Also note that $|v_z| \ll c_s$ implies that the pressure is approximately constant throughout the thermal conduction interface.

The boundary conditions for this equation are $T(z=0) = T_c$, $F(0) = 0$, and that the heating is equal to cooling: $q_+(0) - \Lambda(T_c)n^2(0) = 0$. Analogously, $T(\infty) = T_h$, etc.

Multiplication of equation 6 by the heat flux and integration from $z = 0$ to $z = \infty$ yields

$$\rho v_z = -\frac{I_1}{I_2}, \quad (7)$$

where I_1 and I_2 are the integrals

$$I_1 = \int_{T_c}^{T_h} dT T^{5/2} [q_+ - \Lambda(T)n^2(z)], \quad (8)$$

and

$$I_2 = \frac{5k_B}{2\mu} \int_0^\infty dz T^{5/2} \left(\frac{dT}{dz}\right)^2, \quad (9)$$

respectively. Now, note that I_2 is always positive, and hence the sign of the mass exchange depends only on that of the integral I_1 . Further, the cooling rate is proportional to ρ^2 while the heating rate often is proportional to just ρ , thus for coronal density ρ_h high enough, the radiative cooling forces $I_1 < 0$, and the hot flow will condense. Conversely, for low enough ρ_h , the integral is positive and hence the evaporation is taking place. Evidently, for a given value of T_h a unique value of pressure, at which the mass exchange

is zero, may be defined. This pressure has been termed the ‘‘saturated vapor pressure’’ by Penston & Brown (1970).

Consider now in more detail integral I_1 . Above the peak at $T \simeq 10^5$ in the cooling curve, where $\Lambda(T) \simeq 10^{-21} \text{ erg cm}^3 \text{ sec}^{-1}$, following McKee & Cowie (1977), we approximate the radiative cooling function as $\Lambda(T) \propto T^{-0.6}$ (until the free-free radiation losses become important). Since at a constant pressure $n \propto T^{-1}$, $\Lambda(T)n^2 \propto T^{-0.6}T^{-2} \propto T^{-2.6}$, one could expect that the atomic cooling peak would significantly contribute to the integral. However, the $T^{5/2}$ factor strongly favors high temperatures, and as a result we have $\int dT \Lambda(T)(nT)^2 T^{3/2} \propto p^2 \int dT \Lambda(T) T^{1/2} \propto \int dT \Lambda(T) T^{1/2} \propto T^{0.9}$. This shows that the cooling contribution to I_1 is strongly dominated by the highest temperatures, i.e. by $T \lesssim T_h$. The heating rate is usually a weaker function of temperature and density than the cooling rate, thus the latter statement is even more appropriate. Therefore, approximately, we have

$$I_1 \sim T_h^{7/2} [\bar{q}_+ - \overline{\Lambda(T)n^2(z)}] \propto Q_+ - Q_-, \quad (10)$$

where the vertical bar signifies averaging over the hot flow, and the symbols Q_+ and Q_- are the vertically integrated heating and cooling rates in the corona region.

We shall recall that for typical heating and cooling mechanisms, a two-phase system without a thermal conduction may be thermally unstable over a certain range in pressure (e.g. Field 1965; Krolik, McKee & Tarter 1983). In particular, an initially uniform hot one phase medium will become thermally unstable and develop condensations when a critical pressure value is exceeded. Now, an important point is that this critical pressure and the saturated vapor pressure are usually rather close. For example, in the common Compton-bremsstrahlung case (McKee & Begelman 1990), the critical pressure is 0.95% of the pressure at which thermal instability in the hot gas starts to form clumps. The foregoing discussion and equation 10 explain this result. As the integral I_1 is dominated by temperatures $T \simeq T_h$, thermal conduction drives condensation at approximately same conditions as those when the thermal instability starts to form condensations in the hot flow.

In the context of an accretion flow, the critical pressure or density can be used to define a critical accretion rate, \dot{m}_{crit} . In this paper we measure accretion rates in units of the Eddington accretion rate, defined as $L_{\text{Edd}}/0.1c^2$, where $L_{\text{Edd}} = 1.4 \times 10^{46} M_8 \text{ erg s}^{-1}$, and M_8 is the black hole mass, M_{BH} , in 10^8 Solar masses. In the Non-Radiative Accretion Flow theories (NRAFs, e.g. Narayan & Yi 1994; Blandford & Begelman 1999, BB99 hereafter), the radiative cooling term is not important ($Q_- \simeq 0$) as the gas is very tenuous. However, as the accretion rate increases, gas density increases, the radiative loss term eventually becomes important, and a radiative collapse of the hot (one-phase) flow occurs when $Q_- \simeq Q_+$. The corresponding critical accretion rate, $\dot{m}_{\text{crit}} \sim \alpha^2 r_4^{-1/2}$ (e.g. Narayan & Yi 1995; Esin 1997), where r_4 is radius in units of $10^4 R_S$, with $R_S = 2GM_{\text{BH}}/c^2$, the Schwarzschild radius. The arguments made above for the *classical* thermal conduction show that the critical accretion rate at which the mass exchange in the two-phase flow is zero, \dot{m}_{clas} , is quite close to \dot{m}_{crit} . In a simple model for the two-phase flow with $q_+ = 9/2\alpha\rho c_s^2 \Omega_K (1 - T/T_{\text{vir}})$, where the $(1 - T/T_{\text{vir}})$ approximately accounts for the effects

of winds, and free-free cooling, we found that the conduction drove evaporation at $\dot{m}_{\text{clas}} \approx 0.7\dot{m}_{\text{crit}}$.

Summarizing these results, within the classical heat flux approximation, the hot flow evaporates the cold disk for accretion rates smaller than \dot{m}_{clas} , and condenses for $\dot{m} > \dot{m}_{\text{clas}}$. The classical condensation accretion rate \dot{m}_{clas} is only slightly lower than the critical accretion rate \dot{m}_{crit} at which the hot non-radiative flows without underlying disks would collapse to a thin disk. In the NRAF theories the radiative cooling term is not important, and hence these flows should drive an evaporation of the cold disk.

3 CONDENSATION/EVAPORATION IN COLLISIONLESS LIMIT

3.1 The non-local heat flux

As accretion rate decreases, density decreases in non-radiative accretion flows. Thus at some point λ (equation 4) will become larger than the scale height $H < R$ of the hot flow, and the classical heat flux description will become invalid (the exact condition for this is discussed in §6.1). The common approach in the astrophysical literature is to limit the heat flux to the saturated heat flux value, as described in §2.1. However, although the saturated heat flux prescription remedies the situation as far as the maximum heat flow is concerned, it appears to be unreliable in regard to the correct estimate of the conductive heating rate. Namely, the latter is calculated as $dF_{\text{sat}}/dz = 5\phi P dc_s/dz = 5\phi P (c_s/2T)dT/dz$. While the heat flux is finite in the limit $dT/dz \rightarrow \infty$, the thermal conduction heating is infinite. Physically, the maximum heating rate should be given by the heating rate of a cold test particle immersed in the hot gas (in fact it is far lower than that due to self-generated electric fields).

A detailed calculation of the vertical structure of the transition region between the hot and the cold gas is beyond the scope of the present paper (but will be taken up in Nayakshin & Sunyaev 2004, in preparation; NS04 hereafter). The problem should be clearly treated with a physical kinetic approach rather than a hydrodynamical one. However we can take guidance from the laser-heated plasma (LHP) research, in which the thermal conduction in the collisionless (saturated) regime has been thoroughly studied via direct physical kinetics calculations and *in-situ* experimental measurements. At a physical level, the LHP research showed the importance of the high energy electrons that have very long mean free paths. These electrons carry most of the flux and their distribution function is not coupled to the the average quantities such as the mean temperature.

Luciani, Mora & Virmont (1983; LMV hereafter), and Luciani, Mora & Pellat (1985) were able to formulate a “non-local” heat flux prescription that operates with *hydrodynamical* not physical kinetics quantities, and is yet able to capture the majority of the relevant physics. The price that one has to pay for a greater self-consistency is that the heat flux becomes a non-local quantity. In particular, LMV expressed the heat flux, F_{nl} , as an integral – a convolution of the classical Spitzer’s flux with a kernel that has a width of $\sim \lambda$:

$$F_{\text{nl}}(z) = \int_{-\infty}^{+\infty} \frac{dz'}{2\lambda(z')} F_{\text{cl}}(z') \exp[-\tau(z, z')] , \quad (11)$$

where $\tau(z, z')$ is the “electron optical depth” between location z and z' ,

$$\tau(z, z') = \left| \frac{1}{\lambda(z')n(z')} \int_z^{z'} dz'' n(z'') \right| . \quad (12)$$

(Note that λ used by LMV is about a factor of 2 larger than the electron equipartition λ mentioned in §2.1; NS04). Formula 11 has a simple physical interpretation: as the heat flux is dominated by electrons with energy $E \gtrsim 5k_B T$ (e.g. see §IIA in Schurtz et al. 2000 for a nice account of this fact), their behavior is non-local. They are practically free streaming and thus the exponential factor in equation 11 is an attempt to model their transfer.

Formula 11 reduces to the classical limit when $\lambda \ll L_T$, as expected. In addition, the non-local heat flux may be shown to scale as the saturated heat flux² at an infinitely sharp temperature discontinuity, as it should. Most importantly, the heating rate due to the non-local electron conduction – the derivative of F_{nl} (equation 3) – acts now on the kernel underneath the integral sign and hence it is finite.

Although semi-empirical, formula 11 has been checked against numerical Fokker-Planck simulations (starting from Luciani et al. 1985). There have been improvements to the LMV kernel, and new non-local kernels were suggested (e.g. Albritton et al. 1986; also Epperlein & Short 1991, and references there). However they are all based on the same physical ideas, and the LMV approach still remains the most popular choice (e.g. Ditmire et al. 1998; Schurtz, Nicolai & Busquet 2000) perhaps due to its relative simplicity.

3.2 Vertical temperature profile

The expected vertical temperature structure of the two-phase flow with a transition region is shown schematically in Figure 2. The x -axis of the plot shows the column depth from the disk midplane, i.e. $N = \int_0^z dz' n(z')$. The corona is situated on the top and its temperature, $T_h \geq 10^7$ K (may be much hotter, say 10^9 K). At the lower boundary of the hot flow, gas “temperature” rapidly decreases over a thin layer separating the corona from the “conduction heated zone”. In the both the classical and the saturated heat flux theories, almost all of the heat carried by the hot electrons should be dissipated inside the region of the high temperature gradient. As the radiative losses there are small, this heating would be unbalanced and would lead to a vigorous evaporation. However, both the classical and the saturated heat flux formulations fail to describe this region properly. The particle distribution function in the region is strongly non-Maxwellian as it consists of a mix of the hot and the cold particles. While the local “temperature” does define the mean particle kinetic energy, it is not related to the energy dispersion at all. The non-local heat flux predicts that only a small fraction of the heat flux, i.e. $\Delta z/\lambda$, where Δz is the width of the transition zone, will be liberated in the region of the steep temperature gradient. Thus the evapo-

² The normalizing factor ϕ in equation 5 models complicated plasma collective effects, magnetic fields, etc., and may also be introduced in equation 11.

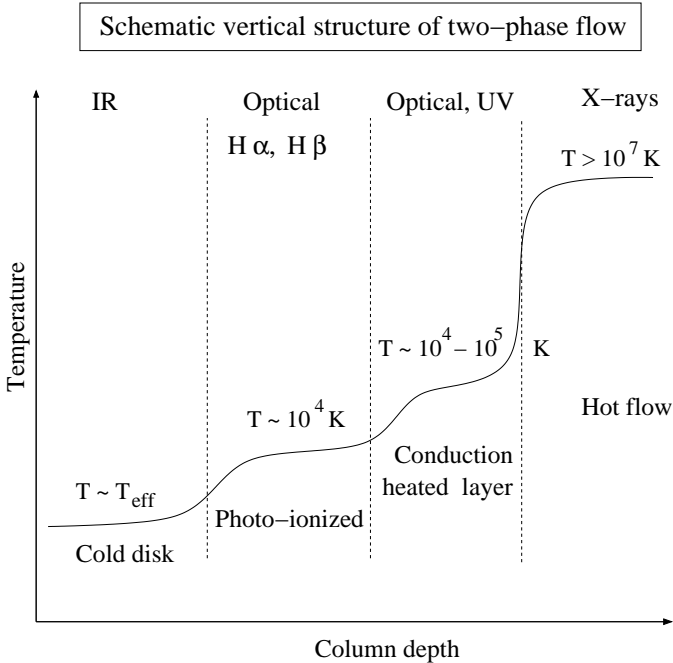


Figure 2. Schematic vertical temperature profile of the two-phase flows (not to scale). The “cold disk” region is the bulk part of the disk. Directly above it is the layer heated and photo-ionized by emission of the gas above it (X-rays and possibly UV). The $T \sim 10^4 - 10^5$ K region is conduction-heated by the energetic electrons penetrating directly from the hot flow. The depth of this layer is of order one mean free path of hot electrons.

ration rate of this region is strongly reduced compared with the saturated heat flux predictions (NS04).

The rest of the non-local heat flux enters the conduction-heated transition layer, in which the particle distribution is dominated by the cold gas, and whose temperature is $\lesssim 10^5$ K as this corresponds to the peak of the optically thin cooling curve. Hydrogen in the layer is collisionally ionized. Below we shall show that the layer is dense enough to re-radiate away the deposited thermal conduction heating. The emission occurs mostly in the optical and UV frequencies. The column depth of the conduction-heated zone is about one penetration depth, i.e. $N_p = \lambda n \simeq 10^4 T_h^2 \text{ cm}^2$. Since the hot flow by definition is optically thin to the hot electrons, the transition layer is actually optically thicker than the latter.

Roughly a half of the radiation emitted by the conduction-heated zone, plus X-rays from the corona, is directed to and penetrate into a deeper cooler layer of the disk, photo-ionizing hydrogen there. This deeper layer is thus essentially an HII region. Finally, yet deeper is the main body of the disk. The disk is assumed to be optically thick and be at least as hot as the effective temperature corresponding to the heat flux from the hot flow ($\sigma_B T_{\text{eff}}^4 \simeq F_{\text{sat}}$).

3.3 Energy balance in the conduction-heated zone

The heating rate due to the non-local electrons penetrating the cold gas from the corona is

$$H_{\text{nl}} = \left| \frac{dF_{\text{nl}}}{dz} \right| = \frac{F_{\text{sat}}}{\lambda_{\text{hc}}} \exp[-\tau(z)] = \frac{5\phi P C_s}{\lambda_{\text{hc}}} \exp[-\tau(z)], \quad (13)$$

where we set the maximum of the non-local heat flux to equal to the saturated heat flux in the corona, at it should; $\tau(z)$ is the optical depth of the hot electrons measured from the bottom of the corona, λ_{hc} is the mean free path of hot electrons *in cold gas*, $\lambda_{\text{hc}} = N_p/n_c$, and n_c is the cold (that is local) gas number density. Note that the heating rate is simply given by the heat flux (F_{sat}), divided by the effective distance to which the hot particles penetrate (λ_{hc}), plus the attenuation factor ($\exp(-\tau(z))$).

Note that everywhere except the hot corona the pressure scale height is much larger than the temperature scale height, and hence the pressure is roughly constant with height (until the top coronal layers). With this, we have numerically

$$H_{\text{nl}} \lesssim 10^{-22} \phi x_e T_5 T_8^{-3/2} n_c^2, \quad (14)$$

where $x_e \leq 1$ is the fraction of free electrons in the transition layer, $T_5 = T_c/10^5$ K is its temperature, and $T_8 = T_h/10^8$ K is the hot flow temperature. Introduction of x_e above is a rudimentary attempt to account for the change in the energy exchange rate, and is approximately valid as long as $x_e \gtrsim [\ln \Lambda_c]^{-1}$. At lower x_e ionization of atomic Hydrogen, rather than Coulomb collisions, becomes the dominant heating mechanism.

The cooling rate of the transition layer is $\Lambda(T_c)n_c^2$. The maximum of the cooling function for collisionally ionized gas is around $\Lambda_{\text{max}} \sim 10^{-21}$ erg/sec cm^3 at temperature $T_c \simeq 10^5$ K (e.g. Raymond, Cox & Smith 1976). Comparing this with the heating rate given by equation 14, we observe that this heating *can* be compensated by the atomic cooling if $T_h \gtrsim \text{few} \times 10^7$ K or so. In addition, the non-equilibrium ionization state of the gas can further increase the cooling function by a factor of up to few tens (e.g., see Fig. 5 in Borkowski et al. 1990). This (i.e. $\Lambda(T)n^2 > H_{\text{nl}}$) is the regime that we are interested in.

It is instructive to compare the cooling rates in the hot corona and in the conduction-heated layer. The former is $\sim 10^{-23} n_h^2$ erg cm^3/sec , whereas the latter is $\sim 10^{-21} n_c^2 = 10^{-21} (T_h/T_c)^2 n_h^2$, i.e. typically some 6-8 orders of magnitude larger. This is why the cold disk is such an efficient coolant for the hot coronal flow.

3.4 Condensation of hot gas

Up till now we have considered thermal conduction due to electrons only. The ion thermal conductivity is neglected in all three formulation – the classical, saturated and the non-local – for the reason that ions are much heavier and thus much slower than the electrons, thus carrying much less flux. However, in the saturated heat flux conditions, the electron heat flow is limited by factors of many to few tens compared with their free-streaming flux, most likely due to charge conservation and plasma instabilities arising when electrons stream past the ions. Thus the ion heat flow may become more important.

Coulomb heating rates of cold gas by hot Maxwellian electrons and ions are well known (Spitzer 1962). In the problem of interest, the situation is far more complex since it is not well known whether and how the non-thermal ions will stream into the cold gas (e.g. see Balbus & McKee 1982). Below we shall make the simplest assumption, namely that the ratio of the non-local ion heating rate of the cold gas

6 *Nayakshin*

to that done by the non-local electrons (equation 13) is the same as that for a Maxwellian distribution. Thus the total ion (assumed to be proton) and electron non-local heating rates are

$$H_{\text{tot}} = H_{\text{nl}} G(T, T_h), \quad (15)$$

where the factor G is (Spitzer 1962; Balbus & McKee 1982):

$$G = 1 + \frac{43 f_p}{(1 + 1836 T/T_h)^{3/2}}. \quad (16)$$

The factor $f_p < 1$ is introduced to parameterize the fraction of the heat flux carried by the ions. Note that $G \rightarrow 1$ for $T \gg T_h/1000$ and that $G \rightarrow 1 + 43f_p$ for $T \ll T_h/1000$. As an example, for $f_p = 0.5$, $T = 10^5$, and $T_h = 3 \times 10^7$ K, $G \simeq 2.2$, whereas for $T_h = 10^8$, $G = 5.5$.

Now, if the fraction of the non-local flux dissipated in the transition layer between the conduction-heated zone and the corona is negligible, and if $\Lambda(T)n^2 > H_{\text{tot}}$, condensation will prevail over evaporation. Since G is not much larger than unity for $T_h \lesssim 10^8$ K, and since for larger T_h the total heating rate decreases as $T_h^{-3/2}$ (equation 14), it appears that the condensation will be taking place when the corona temperature is larger than the ‘‘condensation temperature’’ $T_{\text{cond}} \sim 10^7$ K.

It is likely that the hot flow temperature at the outer radius R_0 (see §4.1) is nearly virial. The latter exceeds T_{cond} for radii smaller than $\sim 10^5 R_S$, i.e. in most astrophysically interesting situations (e.g. cf. Fig. 5 in Narayan 2002). Also note that X-ray spectra of LLAGN are usually power-laws in 2-10 keV energy band, and thus on purely observational grounds the temperature of hot flows should be larger than 10^7 K for these.

4 RADIAL DYNAMICAL EQUATIONS FOR HOT FLOW

We now wish to write down simplified equations for the hot condensing flow with a goal of providing an example of the radial structure of such flows. We shall do this only for the newly found non-local condensation regime (§3), when the heat flux is saturated.

4.1 Domain of applicability in radius

We study the problem at radii smaller than $R = R_c$ where R_c is the circularization radius of the hot gas. For one-phase accretion flows, the radial inflow velocity (e.g. see §5 Frank, King & Raine 2002) of the hot flow is $v_R \sim \alpha c_s (H/R)^2 \sim \alpha c_s$ (for $H/R \sim 1$). Using this we obtain an estimate of the coronal gas density n at any radius R and a given accretion rate. We then compare the hot electron mean free path with R :

$$\frac{\lambda}{R} \sim 0.1 \alpha \dot{m}^{-1} r_4^{-3/2} \quad (17)$$

where $\dot{m} = \dot{M}/\dot{M}_{\text{Edd}}$ is the dimensionless accretion rate ($\dot{M}_{\text{Edd}} = L_{\text{Edd}}/\epsilon c^2$, $\epsilon = 0.1$ is the efficiency of standard accretion, and L_{Edd} is the Eddington limit), r_4 is radius in units of $10^4 R_S$, with $R_S = 2GM_{\text{BH}}/c^2$, the Schwarzschild radius for BH of mass M_{BH} . Estimate 17 was made assuming that the gas is at virial temperature ($T_{\text{vir}}(R) \equiv GM_{\text{BH}}m_p/2k_B R = 2.7 \times 10^{12} r^{-1}$ K; $r \equiv R/R_S$).

According to equation 17, if $\lambda > R$ at some radius R , then it is also true for all internal radii unless the accretion rate \dot{m} increases faster than $\propto r^{-3/2}$ with decreasing R . Barring that, one can define saturation radius, R_{sat} , via condition $\lambda/R = 1$:

$$R_{\text{sat}} \simeq 2 \times 10^3 R_S \left[\frac{\alpha}{\dot{m}} \right]^{2/3}. \quad (18)$$

Below we shall explicitly assume that the heat flux is saturated. The domain of applicability of our solutions is thus $R \leq R_0$, where

$$R_0 \equiv \min[R_c, R_{\text{sat}}]. \quad (19)$$

Formally, our treatment is valid only for non-relativistic electrons. However, for such high temperatures the electron mean free path in the cold gas is so large that its exact value does not particularly matter as long as most of the heat flux is liberated deep in the cold gas and is re-radiated away, allowing condensation of the hot gas.

4.2 Geometry and assumptions

The hot flow is sandwiching a very cold and thin disk located in the midplane (see Figure 1). As already discussed in §3, a very thin (compared with R) transition layer develops between the corona and the conduction-heated layer of the disk. For our present purposes it is sufficient to approximate both the disk and the layer as infinitely thin. Since the cold disk viscous time is very long, the disk can be treated as stationary. Under these assumptions the transition layer and the disk enter the dynamical equations for the hot flow as boundary conditions only.

Due to thermal conduction into the disk, we expect the hot corona to be cooler than ‘‘normal’’ NRAFs that are approximately at the virial temperatures far from the inner flow region (e.g. BB99; Narayan 2002). This makes the thermal pressure gradient not important in the radial momentum equation. The hot flow is thus in a roughly Keplerian rotation. Similarly, thermally driven winds are weak.

4.3 Equations for the hot flow

We now write *height-integrated* equations for a hot rotating flow with a possible mass exchange. Our equations are best understood in comparison with those of the well known solution obtained by Narayan & Yi (1994; hereafter NY94; see their eqs. 1-4), and the equations of MMH94. We begin with the mass conservation equation. In a one-phase accretion flow with no winds or mass deposition, the equation is written as $\partial/\partial R [RH\rho v_R] = 0$, or $\dot{M}(R) \equiv 4\pi RH\rho v_R = \text{const}$. Here $\dot{M}(R)$ is the radial accretion rate, v_R is the radial flow velocity ($v_R > 0$ for accretion), ρ is the height-averaged density in the hot flow. The vertical scale height H is introduced through the hydrostatic balance as $H = c_s/\Omega_K$ where Ω_K is the Keplerian angular velocity. Taking into account the exchange of mass in the vertical direction, the mass conservation equation is:

$$\frac{\partial}{\partial R} [RH\rho v_R] = \rho v_z R, \quad (20)$$

where z is vertical coordinate with $z = 0$ at the cold disk midplane. Since the radial pressure term is small, the radial

momentum equation (eq. 2 in NY94) is trivially satisfied. As the cold disk is also Keplerian, there is no exchange of specific angular momentum between the two flows and the angular momentum conservation equation (3 in NY94) is unaltered. With $\Omega = \Omega_K$ we get

$$\dot{M} = 4\pi R H \rho v_R = \frac{12\pi\alpha}{R\Omega_K} \frac{\partial}{\partial R} [\rho c_s^2 R^2 H] . \quad (21)$$

The entropy equation should include (in addition to the usual terms) the thermal conduction flux, F_{sat} , and the hydrodynamical flux of energy in the vertical direction. In the limit of subsonic vertical flows, $v_z^2 \ll c_s^2$, we write

$$Q_+ + \rho v_z \left[\frac{5}{2} c_s^2 + \frac{GM_{\text{BH}}}{2R} \left(\frac{H}{R} \right)^2 \right] = Q_- + F_{\text{sat}} . \quad (22)$$

On the left hand side of the equation, Q_+ is the vertically integrated viscous heating, and the second term is the mechanical energy flow in the vertical direction. Q_- is the integrated radiative cooling inside the corona:

$$Q_- = \Lambda(T_h) \left(\frac{\rho}{\mu} \right)^2 H \quad (23)$$

where $\mu \simeq m_p$, T_h is the temperature of the hot flow, and $\Lambda(T_h)$ is the usual optically thin cooling function. The cooling term due to the thermal conduction is just the saturated thermal conduction flux, F_{sat} .

Our entropy equation (22) is the height-integrated version of that in MMH94 (see their equation 8), with the following exceptions. As explained in §4.2, we neglect winds here because we are mostly interested in cooler condensing solutions. Thus their side-way expansion term, important for $z \gtrsim R$ (see their eq. 5), is not included. Hence the last term on the right hand side of equation 8 in MMH94 is neglected. The radial entropy flow term (the third line in equation 8 in MMH94) is neglected for the same reason as winds. For Keplerian rotation, the conversion of gravitational energy into heat by α viscosity yields the following heating rate,

$$Q_+ = (9/2) \alpha \rho c_s^3 . \quad (24)$$

It is important to note that both the viscous heating and the thermal conduction cooling (equation 5) scale linearly with ρc_s^3 . After some simple algebra and using $GM_{\text{BH}} H^2 / 2R^3 = c_s^2 / 2$, we find from equation 22 that the condensation velocity is

$$v_z = \left\{ \mathcal{M}_c + \frac{\Lambda(T_h) \rho H}{3\mu^2 c_s^3} \right\} c_s , \quad (25)$$

where \mathcal{M}_c is the Mach number of the condensation velocity in the important limit of negligible radiative losses:

$$\mathcal{M}_c = \frac{5}{3} \phi - \frac{3}{2} \alpha . \quad (26)$$

Note that had we not neglected radial advective cooling, then writing it as of $Q_{\text{adv}} = f_{\text{adv}} Q_+$, where $f_{\text{adv}} \leq 1$ is a parameter (NY94), the only necessary change to equation 26 would be to change $\alpha \rightarrow \alpha(1 - f_{\text{adv}})$.

We will be interested in the parameter space in which $\mathcal{M}_c > 0$, i.e. condensation rather than evaporation. Nevertheless, note that in the opposite limit equations 25 and 26 are not very accurate because we neglected winds. If $\alpha \gtrsim \phi$, the viscous heating dominates the energy balance, the flow is hotter, and it is unlikely that the winds can be rightfully

neglected. The outflowing wind could simply carry the extra heat away thus evaporating the hot flow itself (as in the BB99 solution) but not the cold disk.

4.4 Boundary conditions

At $R = R_0$, we set gas temperature $T_h(R_0)$ to a given (≤ 1) fraction of the virial temperature there. The density at R_0 is determined from a given $\dot{M}(R_0)$ value once $v_R(R_0)$ is found. Since $F_{\text{sat}} \propto p$, the gas pressure, we set $F_{\text{sat}}(z = H) = 0$ in equation 22. As we neglect the mass outflow from the top of the corona to infinity, we also write $\rho(z = H) v_z(z = H) = 0$. The value of the $v_z(z = 0)$, i.e. at the bottom of the corona, is to be found from equations rather than prescribed.

5 APPROXIMATE ANALYTICAL SOLUTION

The first term in equation 25 is a constant while the last one is proportional to density of the flow, becoming small at low accretion rates. We shall thus neglect this term in the non-radiative limit (see §6). Inserting $v_z = \mathcal{M}_c c_s$ into equation (20) and also substituting v_R on its value found from equation (21), we arrive at a second order differential equation that contains two unknown variables, ρ and c_s :

$$\rho R \mathcal{M}_c c_s = 3\alpha \frac{\partial}{\partial R} \left\{ \frac{1}{R\Omega_K} \frac{\partial}{\partial R} \left[\rho c_s^3 \frac{R^2}{\Omega_K} \right] \right\} . \quad (27)$$

This equation cannot be solved analytically or numerically in a general case. By introducing $v_z \neq 0$ we added an extra variable to the accretion flow equations, and the number of independent equations is now smaller than the number of unknowns. This situation is well known in analytical NRAF solutions where one has to introduce three free functions to obtain a solution (BB99). In our case there is no specific angular momentum exchange between the flows, and the heat flux is specified by F_{sat} , therefore we need to parameterize “only” one physical quantity. We have certain well motivated expectations about the radial temperature dependence. For example, for a pure non-radiative flow such as a NRAF with no thermal conduction cooling, $T_h(R) \propto R^{-1}$ for large radii. On the other hand, thermal conduction tends to smooth out temperature gradients (for example within supernova remnants), and hence in the other extreme³, $T_h(R) \simeq \text{const.}$ Thus, we set $c_s = c_0 (R_0/R)^d$, where $0 \leq d \leq 1/2$ and c_0 is the sound speed at R_0 .

If we define $u \equiv \sqrt{R/R_0}$, then equation (27) can be re-written as

$$\rho u^{3-2d} = \frac{3\alpha}{4\mathcal{M}_c} \frac{R_0 c_0^2}{GM_{\text{BH}}} \frac{\partial^2}{\partial u^2} [\rho u^{7-6d}] . \quad (28)$$

Finally, defining $\tilde{\rho} \equiv \rho u^{7-6d}$, we obtain

$$\frac{\partial^2 \tilde{\rho}}{\partial u^2} = \frac{1}{l_c^2} \frac{\tilde{\rho}}{u^{4(1-d)}} . \quad (29)$$

Here l_c is the dimensionless “condensation length”:

$$l_c^2 \equiv \frac{3\alpha}{4\mathcal{M}_c} \frac{c_0^2 R_0}{GM_{\text{BH}}} = \frac{9\alpha}{20\phi - 18\alpha} \frac{c_0^2 R_0}{GM_{\text{BH}}} . \quad (30)$$

³ In fact we first studied the problem via numerical simulations in which we indeed observed this nearly constant $T_h(R)$

We are mostly interested in the case $\phi \gtrsim \alpha$ and therefore we shall only explore the $d = 0$ case below.⁴ In addition, if $\alpha \ll \phi$, the condensation length is small, i.e. $l_c^2 < \alpha/\mathcal{M}_c \sim \alpha/\phi \ll 1$. This circumstance facilitates finding an approximate analytical solution for equation (29):

$$\tilde{\rho} = \text{const} \exp\left[-\frac{1}{l_c u}\right]. \quad (31)$$

Indeed, $d^2\tilde{\rho}/du^2 = \tilde{\rho}(-2/l_c u^3 + 1/l_c^2 u^4) \simeq \tilde{\rho}/l_c^2 u^4$ due to the fact that $1/l_c u > 1/l_c \gg 1$ for $u < 1$.

Returning to the original variables, we explicitly write down the approximate solution:

$$\rho(R) = \rho_c \left(\frac{R_0}{R}\right)^{7/2} \exp\left[-\frac{1}{l_c} \left(\sqrt{\frac{R_0}{R}} - 1\right)\right], \quad (32)$$

$$v_R = \frac{3\alpha}{2l_c} \frac{c_0^2}{R_0 \Omega_K(R_0)} = \sqrt{\frac{\alpha \mathcal{M}_c}{3}} c_0 = \text{const} \ll c_0, \quad (33)$$

$$\dot{M}(R) = \dot{M}_0 \frac{R_0}{R} \exp\left[-\frac{1}{l_c} \left(\sqrt{\frac{R_0}{R}} - 1\right)\right]. \quad (34)$$

Here ρ_c is the gas density at R_0 , and \dot{M}_0 is the accretion rate at that point. Note that $l_c R_0$ is roughly the radial distance over which the hot flow will condense. At $R_0 - R \ll l_c R_0$, there is little left of the hot flow.

Note also that equation (33) shows that the radial velocity is constant and is substantially smaller than the sound speed since we study cases when both α and $\mathcal{M}_c \ll 1$. Further, for $l_c < 1/2$ (recall that we assumed $l_c \ll 1$), the accretion rate increases with R for all $R < R_0$, as it should for a condensing flow. Also note that the radial flow velocity is small compared with the sound speed and yet it is larger than expected for the usual one-phase hot flows for which $v_{R,\text{visc}} \sim \alpha c_s (H/R)^2 \lesssim \alpha c_s$.

Figure 3 shows \dot{M}/\dot{M}_0 as given by equation 34 for $\phi = 0.2$ and two different values of α , i.e. $\alpha = 0.02$ and 0.1 (solid and dotted curves, respectively). The accretion rates are normalized on their values at $R = R_0$. The horizontal dashed curve shows the case of no mass exchange. Note that for the case of very small α , \dot{m} essentially plunges with radius, whereas for $\alpha = 0.1$ (which is only a factor of 2 smaller than ϕ), $\dot{m} \simeq \text{const}$ for a range or radii before it reaches the exponential decline.

5.1 Spectra from condensing flows

For low luminosity systems, Comptonization in the corona is not important. Therefore we expect the coronal spectra to be dominated by the free-free emission as well as X-ray line emission (at the coronal ionization equilibrium) for $T_h \lesssim 10^8$ K. The single temperature free-free spectrum is thus the hardest one that can be expected here; the photon spectral indices are then $\Gamma \gtrsim 1.4$ or so. The spectra are softer for lower T_h and also in the case when there is a broad distribution of temperatures in the corona.

The maximum transition layer temperature is $T_c \lesssim 10^5$ K. Gas at this temperature is a very efficient emitter of UV

⁴ Nevertheless we note that (i) approximate solutions may be obtained for a general value of d , and (ii) for $d = 1/2$ there is a scale-free solution.

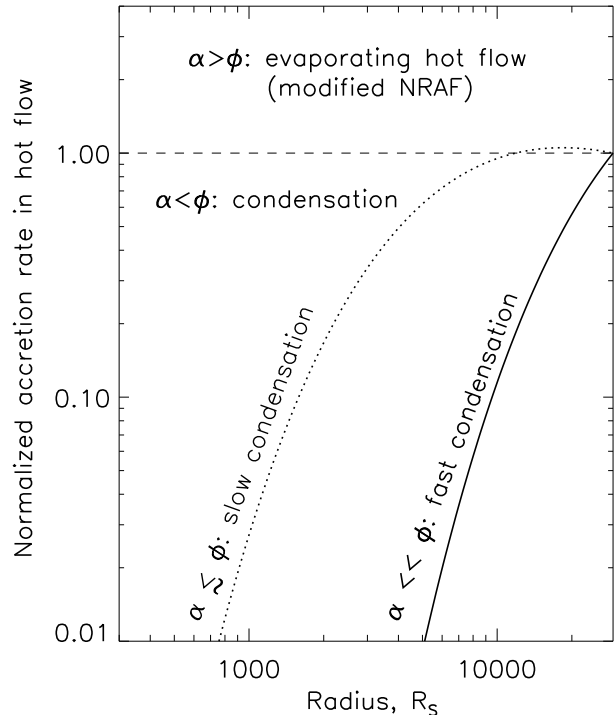


Figure 3. Radial accretion rate profiles in the hot flow normalized on $\dot{M} = \dot{M}(R_0)$ (for $R_0 = 3 \times 10^4 R_S$). The saturated heat flux coefficient is $\phi = 0.2$ for all the cases. The $\dot{M}/\dot{M}_0 = 1$ (dashed) curve shows the case when the hot flow neither evaporates nor condenses, which occurs when $\alpha \simeq \phi$. For α smaller than ϕ , the hot flow is condensing. When α is only slightly lower than ϕ , $l_c \sim 1$, and the condensation is slow (cf. the dotted curve). For $\alpha \ll \phi$, condensation length $l_c \ll 1$, and the hot flow very quickly settles down on the cold disk. This latter case is illustrated by the solid curve for which $\alpha = 0.02$. Finally, for $\alpha \gtrsim \phi$, the hot flow (but not necessarily the cold disk!) evaporates, outflowing to infinity as in the BB99 solutions.

lines, e.g. that of He^+ , Oxygen and other elements. The column depth and thus the emission measure of the gas at $T \simeq 10^5$ K depends on the exact value of the non-local thermal conduction heating, H_{tot} (equation 15), which depends on the hot flow temperature mainly. If the temperature is below $\sim 10^8$ K, then the $\sim 10^5$ K gas will re-radiate a significant fraction of the condensing flow energy. In this case there should be a strong UV bump in the SED of the source, along with another bump of comparable magnitude at the effective temperature of the disk, which is in the infra-red to the optical frequency range depending on the parameters (black hole mass, condensation radius, condensation rate).

If the hot flow temperature is greater than 10^8 K or so at the point where most of the condensation takes place, on the other hand, then the situation is qualitatively different. Since H_{tot} is lower, the layer with $T \sim 10^5$ K exists only due to local thermal conduction and is much thinner than in the opposite case (NS04). Bulk of the conduction-heated zone is at temperature $T \lesssim 10^4$ K. Strong Hydrogen Ly α , H α , H β , etc., line radiation is expected from these layers rather than UV emission. Thus in this case the UV region in the SED of the condensing flow is weak.

As shown in Figure 2, below the conduction-heated layer there will be also a photo-ionized layer, an analog of an

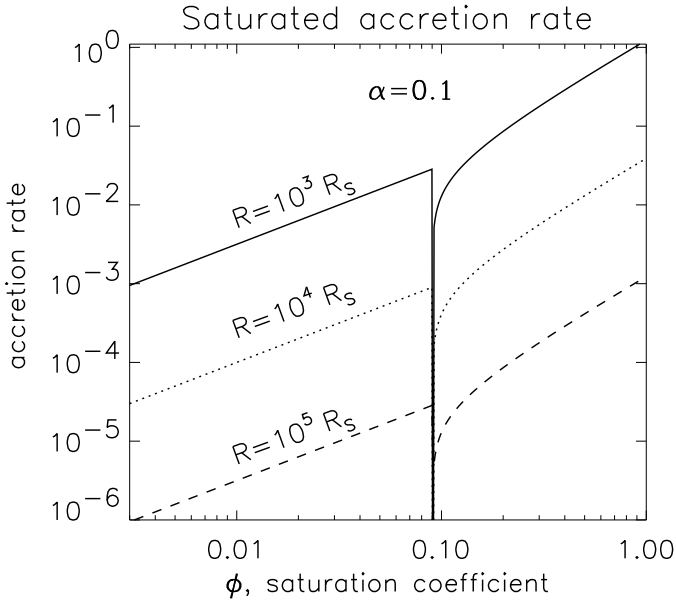


Figure 4. The accretion rate, \dot{m}_{sat} , below which the heat flux in the hot flow is saturated (collisionless), as a function of the saturation parameter ϕ . All the three curves are for $\alpha = 0.1$ but varying radii as labelled above the respective curves. The \dot{m}_{sat} curve is rather approximate in the region $\phi \simeq \alpha$ where the two different limits meet (see equation 35). Note that for the largest radius, the hot flows are saturated only for extremely small values of \dot{m} . On the contrary, for the smallest radius, the hot flows are in the collisionless regime even for relatively large \dot{m} unless $\phi \ll 1$.

HII region. This deeper layer is expected to be a strong emitter of optical lines, especially H α , H β . Therefore note that in the present model the vertical structure of the transition layer contains both collisionally and photo-ionized emission regions whose relative contribution to the optical spectrum will vary depending on conditions.

Finally, below the optically-emitting zone there will be the optically thick cold disk. Its effective temperature will be controlled by both the external energy deposition (the condensing flow plus starlight, etc.) and the internal energy dissipation. For LLAGN, this typically yields $T_{\text{eff}} \sim 10^3$ K.

6 PARAMETER SPACE

6.1 Saturated accretion rate

First we specify the conditions under which the heat carrying electrons in the hot flow are collisionless, i.e. the heat flux is saturated. The estimate is done at radius R_0 , where we assume that the hot flow temperature is virial (in §6.4 we discuss $R < R_0$). Note that for a $\phi < 1$ one has to reduce the electron mean free path λ (equation 4) to $\lambda' \equiv \phi\lambda$. Indeed, the saturation coefficient ϕ is an ad hoc attempt (see Appendix A) to account for the reduction of the electron heat flux due to magnetic fields, plasma instabilities, etc., and to be consistent one should also reduce the electron effective mean free path. The critical gas density can then be related to the accretion rate given that we know the radial velocity of the flow, v_R . For $\phi \gtrsim \alpha$ we use equation 33, whereas for the case of $\phi \ll \alpha$ we can simply neglect the thermal conductivity altogether and use the usual viscous radial velocity

scaling (see the first paragraph in §4.1). Thus we arrive at the following condition for the thermal conductivity of the hot flow to be collisionless:

$$\dot{m} < \dot{m}_{\text{sat}} = \begin{cases} 0.1 \sqrt{\alpha \mathcal{M}_c} \phi r_4^{-3/2}, & \text{if } \phi \gtrsim \alpha \\ 0.1 \alpha \phi r_4^{-3/2}, & \text{if } \phi \lesssim \alpha. \end{cases} \quad (35)$$

Figure 4 shows \dot{m}_{sat} for three different radii and a same value for α -viscosity parameter, $\alpha = 0.1$. The sharp drop in the curves around $\phi \simeq \alpha$ is the artifact of our assumption $\phi \gg \alpha$ that we used to build an approximate analytical solution in §5; in the reality a numerical integration of the equations would yield a smoother transition between the two cases given in equation 35. For radii as large as $10^5 R_S$, the hot flow must be accreting at a dimensionless rate smaller than $\sim 10^{-3} \phi$ for the heat flux to be saturated. However the flow is almost always saturated for “small” radii such as $10^3 R_S$.

6.2 Radiative condensation

As noted in §2.2, spontaneous condensation may be taking place even in an originally one-phase system without any thermal conduction if the in-situ radiative cooling is too large. Hot accretion flows suffer a catastrophic collapse when the cooling exceeds the viscous heating. For a NRAF, this occurs at accretion rates exceeding $\dot{m}_{\text{crit}} \sim \alpha^2 r_4^{-1/2}$ (e.g. Narayan & Yi 1995; although exact results depend on the cooling processes and geometry of the flow: Esin 1997). In the presence of the cold accretion disk below the hot flow, the additional thermal conductive cooling causes the latter to condense at a smaller pressure. In §2.2 we showed that this shifts the value of the critical radiative condensation rate \dot{m}_{rad} downwards by a factor of order unity only, i.e. $\dot{m}_{\text{rad}} \sim \dot{m}_{\text{crit}}$ (but see §6.4 below).

Now, if $\dot{m} < \dot{m}_{\text{sat}}$, i.e. the heat flux is collisionless, and the thermal conductivity is large ($\phi \gtrsim \alpha$), we use the solutions obtained in §5. The radiative cooling contribution to the condensation can be neglected when $\Lambda(T)\rho H / (3\mu^2 c_s^3) \ll \mathcal{M}_c$ (see equation 26). Evaluating this relation at $R = R_0$, assuming the free-free cooling, $\Lambda(T) = 2.4 \times 10^{-27} T^{1/2}$, one finds the accretion rate, \dot{m}_{rad} , at which radiative losses start to dominate the energy balance in the hot condensing flow:

$$\dot{m}_{\text{rad}} = 6\alpha^{1/2} \mathcal{M}_c^{3/2} r_4^{-1/2}. \quad (36)$$

If $\dot{m} < \dot{m}_{\text{sat}}$ but $\phi \ll \alpha$, then the thermal conduction can be neglected and we again estimate that $\dot{m}_{\text{rad}} \sim \alpha^2 r_4^{-1/2}$, as in a pure NRAF case. Combining together these results, we obtain the accretion rate above which condensation is driven by the in-situ radiative losses in the hot flow:

$$\dot{m}_{\text{rad}} = \begin{cases} 6\alpha^{1/2} \mathcal{M}_c^{3/2} r_4^{-1/2}, & \text{if } \phi \gtrsim \alpha \text{ and } F_{\text{cl}} > F_{\text{sat}} \\ \alpha^2 r_4^{-1/2}, & \text{if } \phi \lesssim \alpha \text{ or } F_{\text{cl}} < F_{\text{sat}} \end{cases} \quad (37)$$

6.3 Division of the parameter space

We can now divide the parameter space into different regions by the type of the flow that occurs there. The division is governed by the following principles:

- $\dot{m} < \dot{m}_{\text{sat}}$, $\dot{m} < \dot{m}_{\text{rad}}$, $\phi \gtrsim \alpha$: Non-Radiative Condensation (NRC for short), the solutions obtained in this paper.

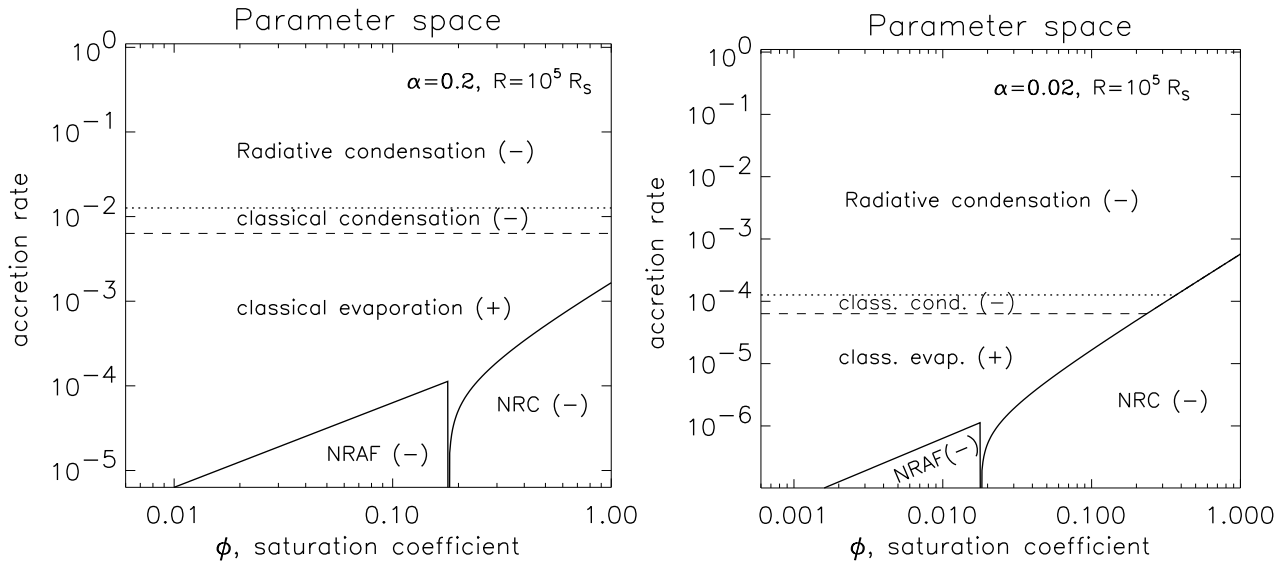


Figure 5. Left panel: The types of solutions occurring in the two-phase accretion flows at radius $R = 10^5 R_S$ and for a “large” value of α -parameter ($\alpha = 0.2$), as a function of the dimensionless accretion rate and the saturation parameter ϕ . The signs + or – reflects the sign of the mass exchange between the disk and the hot flow. See text in §6.3 for a detailed discussion of the Figure. Right panel: same as the Left one but for $\alpha = 0.02$.

- $\dot{m} < \dot{m}_{\text{sat}}, \dot{m} < \dot{m}_{\text{rad}}, \phi \lesssim \alpha$: Non-Radiative Accretion Flow (NRAF), with a weak (since ϕ is small) collisionless condensation. The flow structure is similar to the usual NRAFs except the flow should be somewhat cooler.

- $\dot{m} > \dot{m}_{\text{sat}}, \dot{m} < \dot{m}_{\text{rad}}$ Classical evaporation of the disk by the hot flow (e.g. MMH94). “Classical” reflects the fact that the heat flux is in the classical, collision-dominated, regime.

- $\dot{m} > \dot{m}_{\text{rad}}$: Independently of other parameters, the hot corona is condensing onto the cold disk because of a too strong in-situ radiative cooling.

To illustrate the resulting division in the $\dot{m} - \phi$ parameter space, first consider large radii, such as $R = 10^5 R_S$, and large α (Figure 5, Left panel). For each of the segments in the parameter space, the respective type of solution is indicated, and the signs “+” or “–” indicate the sign of the mass exchange between the cold disk and the hot flow; “+” stands for the evaporation of the cold disk.

At the largest accretion rates (above $\dot{m} \simeq 0.01$), the flow condenses due to the radiative losses in the hot flow itself. Slightly below that there is a narrow zone of the classical condensation, which is enabled by the radiative losses inside the hot flow and the transition region.

At yet lower accretion rates, the radiative cooling in the hot flow and the transition layer becomes too weak. The excess energy is used to evaporate the cold disk, as first discussed by MMH94. The hot flow also drives a thermal wind to infinity (MMH94), and in many respects is similar to the NRAF solutions (e.g. BB99; Narayan 2002), although the two-temperature assumption typical for NRAF is not required for these evaporating flows.

Next, below $\dot{m} = \dot{m}_{\text{sat}}$, lie the parameter space where the heat flux is collisionless. As we found in this paper, as long as $T_h \gtrsim T_{\text{cond}}$, the heating of the transition layer by the hot electrons can be counter-balanced by the local radiative losses, and thus the hot flow is condensing. When $\phi \gtrsim \alpha$,

the approximate solutions developed in §5 apply. The hot flow is condensing due to radiative cooling in the transition layer. Unlike the classical condensation regime, however, the transition layer is very much cooler in this case ($T \lesssim 10^5$ K; see §3), and the hot electrons are in a free-streaming collisionless regime. The hot flow can be completely quenched (terminated) in this regime as $\dot{M}(R \rightarrow 0) \rightarrow 0$.

Finally, at $\phi \lesssim \alpha$ and $\dot{m} < \dot{m}_{\text{sat}}$, we have an analog of a hot non-radiative corona that we simply call a NRAF (although once again, it does not have to be a two-temperature flow as such). While the hot flow is still condensing in this case, the process is slow since $\phi < \alpha$, and thus the hot flow will not be terminated as in the NRC case. Therefore, the NRAF (–) case may be quite analogous to the usual NRAFs except for the additional (weak) cooling and condensation provided by the thermal conduction.

Consider now smaller radii (e.g., $R = 10^3 R_S$ in Figure 6). The hot flow is now much hotter, and thus the column depth penetrated by hot electrons is much larger. Therefore the flow is much more likely to be in the collisionless regime. For sufficiently small radii, the hot flow can be both collisionless and radiative along the line separating the radiative condensation and the NRC solutions in the upper right corner of both panels in Figure 6. This means that for such small radii the classical evaporation regime completely disappears for large values of ϕ . As can be seen in Figure 6, for $\phi \gtrsim \alpha$, the hot flow condenses for any \dot{m} , either due to in-situ radiative losses (high \dot{m}) or due to radiative losses in the transition layer (low \dot{m}) as discussed in §§ 3 & 5.

6.4 On global nature of realistic two-phase flows

As stated in the beginning of §6, so far we have only considered the parameter space for condensation or evaporation at the outer radius of the hot flow, $R = R_0$, where we assumed $T_h = T_{\text{vir}}$. However at smaller radii, where the radial (in-flow) velocity significantly decreases compared to the free-

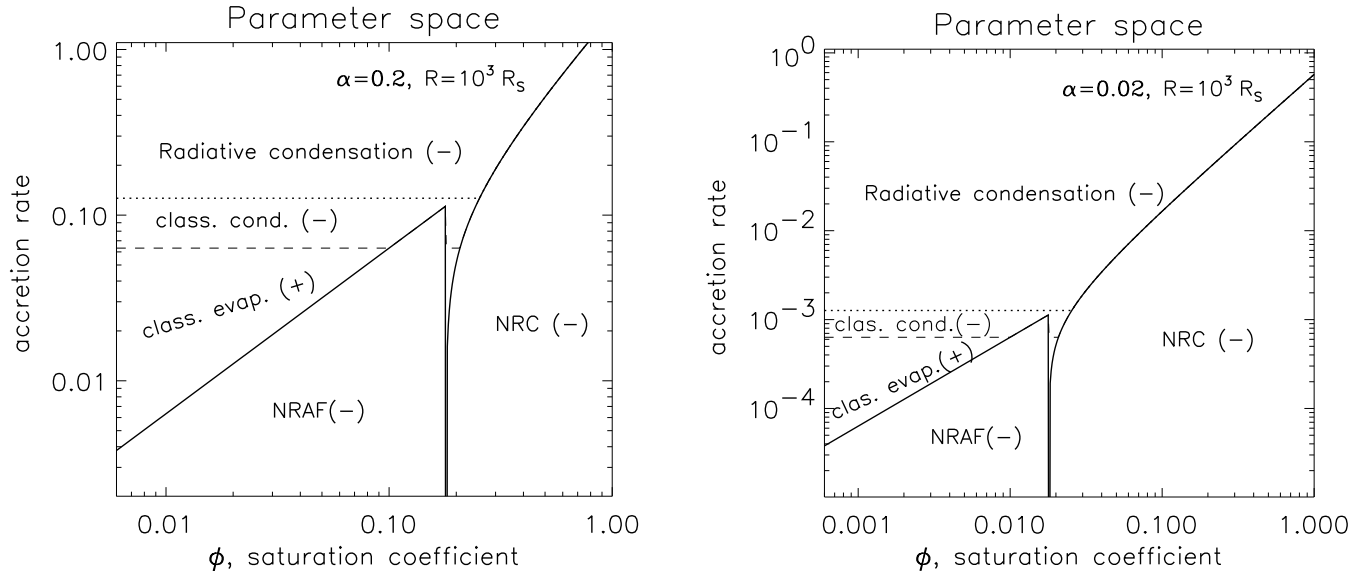


Figure 6. Same as Figure 5, but for $R = 10^3 R_S$. Note that because of the much higher virial temperature at $R = 10^3 R_S$, the thermal conductivity in the hot flow is collisionless for much larger accretion rates than in Figure 5. Thus the region of applicability of the NRC solutions grows, while the “classical evaporation” zone shrinks.

fall value, one expects that the thermal conduction will be much more efficient in cooling the hot flow to $T_h \ll T_{\text{vir}}$.

Let us determine how the value of \dot{m}_{rad} changes in this case. The integrated heating rate, Q_+ , is the rate at which the inflowing gas liberates its gravitational energy, and hence it only depends on the accretion rate, \dot{m} , and is independent of the coronal temperature. The radiative cooling rate, however, scales as $Q_- \sim \Lambda(T_h)\rho^2 H$. Since $H/R \simeq \sqrt{T_h/T_{\text{vir}}}$ for accretion flows, and $v_R \simeq \alpha\Omega_K R(H/R)^2$, we have $\rho \propto \dot{m}(T_{\text{vir}}/T_h)^{3/2}$. Taking $\Lambda(T_h) \sim \text{const}$, we see that the radiative cooling rate approximately equals the heating rate at

$$\dot{m}_{\text{rad}} \sim \alpha^2 r_4^{-1/2} \left(\frac{T_h}{T_{\text{vir}}} \right)^{5/2}, \quad (38)$$

which may be significantly smaller than that given by equation 37. Evidently, the influence of the thermal conduction on the collapse of a hot flow is very significant in this example in the cumulative sense. While a hot one-phase accretion flow with $T_h \simeq T_{\text{vir}}$ may be thermally stable to collapse (spontaneous condensations), the two-phase hot flow with same accretion rate would be much cooler, $T_h \ll T_{\text{vir}}$, much denser, and would thus collapse onto the cold disk. The detailed calculations by Liu et al. (2004) show that this is exactly the case. These authors find a condensing solution for $\alpha = 0.1$ and accretion rate $\dot{m} \sim 3 \times 10^{-3}$, which would be somewhat too low for the classical condensation. However their vertical temperature profiles show that the coronal temperature is only $T_h \sim 0.3T_{\text{vir}}$, making $\dot{m} < \dot{m}_{\text{rad}}$ according to equation 38, and enabling condensation.

Even more complex situation may exist when the gas is evaporating at large radii but condenses at small radii, or the flow is in the classical thermal conduction limit at large radii and is yet in the saturated conduction limit at small R . This complexity of the two-phase flows with thermal conduction is not something new, however, as accretion flow equations are well known to allow more than one self-

consistent solution at same \dot{M} and radius (e.g. Abramowicz et al. 1995).

7 APPEARANCE OF CONDENSING FLOWS

From the disk ionization instability theory (for reviews see Cannizzo 1998, Lasota 2001), it is well known that “cold” accretion disks may be in two states: (i) active, that is accreting, in which case the disk is approximately in a steady state, with the accretion rate equal to a constant independent of radius. (ii) quiescent or inactive, when most of the hydrogen is neutral. The disk then accumulates the mass and the accretion rate strongly decreases with decreasing radius R .

In the case of an active disk, we expect that a steady-state will be reached in which the mass deposited by the condensing flow is accreted with time onto the black hole. The luminosity of the inner accretion flow is then much larger than that of the condensing flow at large radii. Accordingly, the latter is a minor detail in the overall spectrum of the source. This situation is more likely to realize for the classical thermal condensation that takes place at a relatively high accretion rate than the non-radiative condensation.

In the opposite case of a quiescent disk, the situation is completely different since then the luminosity of the system is much smaller and the condensing flow may be the primary radiation source. This astrophysically interesting case is more likely for the non-radiative condensation, and is discussed below.

7.1 Underluminous accretion flows

If the cold disk is inactive, i.e. barely accreting, in analogy to quiescent disks in binary transient systems (e.g. see Cannizzo 1998; Lasota 2001), then the mass condensing on it

may be stored there for very long times. Indeed, the viscous time scale at radius R is

$$t_{\text{visc}} \sim 3 \times 10^8 \text{ years} \frac{M_8 r_4^{1/2}}{\alpha_2 T_3}, \quad (39)$$

where M_8 is the black hole mass in units of 10^8 years, α_2 and T_3 are the cold disk viscosity and the temperature in units of 0.01 and 10^3 Kelvin, respectively. For example, for Sgr A*, with $M_8 \sim 0.03$ and with $T_3 \sim 0.1$ (e.g. Nayakshin et al. 2004), this corresponds to 10^8 years, far longer than the age of the bright young stars estimated at $\lesssim 10^7$ years (e.g. Ghez et al. 2003). For a black hole mass of $\sim 10 M_\odot$, $t_{\text{visc}} \sim 30$ years, a time relatively long for binary systems.

For inactive disks, the accretion rate through the inner boundary, \dot{M}_i , is much smaller than that at large radii (e.g. Nayakshin & Svensson 2001), \dot{M}_0 . Some rough estimates are possible. Suppose the condensing gas is deposited onto a ring with radius $R = R_0$, and that the initial mass of the cold disk, $M_d(t=0)$, is negligible small. Thus the disk mass at time t is $M_d(t) \simeq t\dot{M}_0$. The time needed for the matter to diffuse to the innermost stable orbit is exactly the viscous time. The rate at which the black hole consumes the disk can be estimated as (see, e.g., §5 of Frank et al. 2002)⁵

$$\dot{M}_i(t) \sim \frac{M_d(t)}{t_{\text{visc}}} \exp\left[-\frac{t_{\text{visc}}}{t}\right] \sim \dot{M}_0 \frac{t}{t_{\text{visc}}} \exp\left[-\frac{t_{\text{visc}}}{t}\right]. \quad (40)$$

This equation shows that as long as $t \ll t_{\text{visc}}$, the innermost accretion rate is very small compared with that of the hot condensing flow. The expected luminosity of the innermost disk is $L_i \sim 0.1\dot{M}_i c^2$. Comparing this with the luminosity of the condensing flow at $R = R_0$, $L_{\text{cond}} \sim (3R_S/R_0)0.1c^2 \dot{M}_0$,

$$\frac{L_i(t)}{L_{\text{cond}}} \sim \frac{\dot{M}_i(t)}{\dot{M}_0} \frac{R_0}{3R_S} \sim \frac{R_0}{3R_S} \frac{t}{t_{\text{visc}}} \exp\left[-\frac{t_{\text{visc}}}{t}\right]. \quad (41)$$

Even if $R_0 \gg 3R_S$, the luminosity of the inner disk is small as long as $t \ll t_{\text{visc}}$.

Therefore, we see that the hot condensing flow in couple with an inactive cold disk are “underluminous” when compared with accretion flows that carry the gas directly into the black hole (i.e. assuming the standard 10% efficiency of the mass to radiation conversion for accretion). The effect is of course a time dependent one; upon averaging over $t \gg t_{\text{visc}}$, the average luminosity of the two-phase flow equals that of the standard accretion flow (Shakura & Sunyaev 1973).

7.2 Missing or truncated inner disks

If the cold disk is truly inactive, only the area of the disk actually covered by the hot flow will be emitting. If one estimates the disk extent via the velocity width of H α line or via the SED of the source, then it may appear that there is no disk at small radii because most of the hot flow does not reach there. While it is quite possible that the inner disk is missing altogether, it may also be in the inactive state where it emits very little to be detectable, as explained above.

⁵ Exact results will depend on the run of the cold disk temperature with radius, but the dominant exponential factor will be always similar

7.3 SED for non-radiative condensation

In the two-phase flows studied here, most of the thermal energy resides in the hot corona. However, in the non-radiative case, the corona is cooled by thermal conduction instead of radiation. Owing to this, the radiation output of the condensing flow is dominated by the radiation of the underlying disk. X-ray emission for such flows should always be weak compared with the thermal-like bump in the infrared to UV frequency region (depending on the black hole mass and other parameters).

7.4 SED for radiative condensation

If the hot gas condensation is initiated by the radiative losses in the corona itself (§2), then most of the hot flow energy is emitted in X-ray frequencies. Barring the case of a very optically thin cold accretion disk, about half of this radiation is absorbed in the disk and is re-emitted in the infra-red and/or optical frequencies. Thus in this case the SED of the source should contain a similar amount of power in the X-ray and the disk components.

Clearly, a case intermediate between this and that considered in §7.3 exists, when the hot flow persists for a decade or more in radius before succumbing to the condensation process (see end of §6.4).

7.5 Broad double-peaked emission lines

As we discussed in §5.1, the gas sandwiched between the corona and the cold disk is a strong emitter of optical and UV (if hot enough) lines. X-rays from the corona also contribute to radiative ionization and emission of optical/UV lines. Also note that the hot completely ionized coronal gas, settling down on the disk, will have to recombine, again producing emission lines. Therefore a generic prediction of our model is the presence of strong emission lines that should be shifted and broadened due to disk rotation, resulting in double-peaked line profiles. We expect the lines to trace a broad range of conditions and hence be a mix of photo-ionized and collisionally ionized cases.

7.6 Fluorescent Fe K α lines

Here we have considered the hot X-ray emitting flow at large ($R \sim 10^3 - 10^5 R_S$) distances from the black hole. If such a flow condenses and liberates most of its energy at these large distances, when clearly any Fe K α line due to reprocessing of the radiation in the cold disk would be “narrow”, in accord with the observations (e.g. Ptak et al. 2004; Dewangan et al. 2004). Furthermore, because the inactive disks may be powered by condensation of the hot gas rather than by the internal disk accretion, the column density of these may be much lower than that deduced from the cold disk equations with the accretion rate tuned to match the optical/UV output of the source. Thus the inactive disks studied here may actually be Thomson-thin, producing no detectable Fe K α line at all.

8 CONCLUSIONS

Here we studied the physics by which a hot flow above a cold accretion disk could condense. Such a condensation process is of a large practical importance for accretion in AGN and X-ray binaries. Without means to cool, the hot gas is an extremely inefficient kind of fuel for the black hole (e.g. BB99). Not only the gas radiates little, it also *accretes* little (for recent numerical simulations see Proga & Begelman 2003). In contrast, if the hot gas condenses onto a cold accretion disk, the gas may temporarily lose its viscosity, i.e. the ability to accrete efficiently, but it remains tightly bound to the black hole. With time, when accretion through the cold disk is restarted, the hot gas will accrete onto the black hole. Thus our condensing scenario for the accretion of the hot gas onto the black hole is much more efficient in feeding the hot gas into the black hole than the non-radiative hot flows (BB99, Narayan 2002).

We have found two distinct condensation regimes: (i) radiative or classical, which takes place when the radiative cooling term in the corona is comparable with the viscous heating term (see §2) and the thermal conductivity is classical; and (ii) non-radiative. When the flow density is very low and the radiative losses are negligible. However the hot particles have very long mean free paths that allow them to penetrate the cold gas directly. Their energy is then re-radiated by the dense cold layers (see §3). The cold disk thus serves as a cooling plate, radiator, for the hot flow. This second condensation regime is not expected based on the previous literature that employed the classical or the saturated heat flux formulations.

We also presented a simple analytical solution describing the radial structure of the hot flow for the non-radiative condensation. The solution is obtained under the assumption of hot flow temperature constant with radius and is meant to be an example only. The detailed structure of the flow is not as important for the flow energetics as long as one can clearly define a radius R' where most of the corona condenses. As the hot gas condenses, the gravitational energy released per unit mass of hot gas is $\sim GM_{\text{BH}}/2R'$. If the cold disk is inactive, then most of the condensed mass is stored in the disk until the disk becomes massive enough (e.g. Siemiginowska, Czerny, & Kostyulin 1996; but note that galaxy mergers, etc., may be another “direct” way of triggering accretion outbursts in the inner parsec from the BH). Thus the luminosity of the condensing flow (while the disk is inactive) is quite small compared with that expected for standard accretion flows (§7.1).

Nuclei of LLAGN is an example where the two-flow geometry is natural – e.g. see Fig. 2 of Ho (2003) and note that in reality the hot gas probably fills the whole available space because it is too hot to be confined (BB99). Currently, the bump-like infra-red feature seen in the SED of LLAGN is thought to be due to the *accretion* through the disk. Assuming that the flow in the disk is continuous down to the last stable orbit however leads to a paradox since then one would expect a far brighter source. In contrast, if the cold disk is powered by the condensing corona and there is no accretion in the disk itself, there is then no problem with the source being too dim. The current “non-radiative” condensation mechanism is thus somewhat inconspicuous in that the radiative output of such a flow is dominated by the emission

of a warm atomic and ionized gas and not by the energy source – the hot gas.

A similar picture may be relevant for quiescent disks in transient binary systems if not all of the accretion stream radiatively condenses in the hot spot (the hot spot emission is quite weak in many systems; see references in Lasota 2001, his §7). Thus in some systems the “disk” continuum and line emission may be excited by shocks in the hot spot, whereas in others (with a weaker hot spot), the emission may be produced by the diffuse hot flow condensing onto the disk.

Since the accretion flow may span a broad range of radii, it is possible that different types of mass exchange solutions realize at different radii. For example, at a high enough accretion rate, the hot flow may be condensing radiatively at large radii, whereas at small radii, where the accretion rate is significantly reduced, it may condense by the non-radiative mechanism. It is equally possible for the accretion flow to be evaporating at large radii and condensing at small ones. Therefore we should keep in mind that in general a mix of the solutions is possible. This “unfortunate” multi-phase complexity of accretion flows is not something unique to the accretion process; after all the interstellar medium has a multi-phase structure too.

Finally note that due to processes not taken into account in the standard disk instability model (e.g. Cannizzo 1998), for example photo-ionization of the disk upper layers by starlight and X-rays; stellar impacts (Nayakshin et al. 2004), etc., there will always be a finite (weak) accretion onto the BH. This weaker accretion may power the jet emission.

Our results also indicate that a left alone cold disk will *not* necessarily have to evaporate into a hot corona at a low \dot{m} via the classical thermal conductivity (MMH94). Indeed, when a hot corona just starts developing above the disk, the coronal accretion rate initially is very low and it is thus in the collisional, not classical, regime.

9 ACKNOWLEDGMENTS

We thank Rashid Sunyaev for his careful reading of an earlier draft of the paper, and the many useful suggestions and comments that he made that substantially improved this work. We also acknowledge very useful discussions with F. Meyer, E. Meyer-Hofmeister, B. Liu, H. Spruit & K. Dullemond. Finally, C. McKee is thanked for several illuminating discussions during the author’s visit to UC-Berkeley.

APPENDIX A: NOTES ON COMPLICATIONS NOT CONSIDERED HERE

Magnetic fields Magnetic fields are not explicitly introduced in this paper. The reason is pragmatic – magnetic fields in accretion flows are known to be turbulent and time-dependent (e.g. Balbus & Hawley 1991) and there seems to be no hope of obtaining an analytical solution such as that found in §5 when thermal conduction and fields are both considered. The presence of even a very weak (far sub-equipartition) magnetic field strongly reduces the thermal conductivity in direction perpendicular to the field lines. The usual approach is to set the conductivity to zero in that

direction (e.g., see Balbus 1986). Thus, the effective value of ϕ will be reduced by any non-zero magnetic field, but an essential point is that *this reduction is a function of the field topology but not the field strength*. The main unknowns in this regard are the field correlation length and the angular distribution of the field directions near the interface between the hot and the cold flows.

The value of the effective viscosity coefficient α is also a function of the magnetic field, but *a different function*. While the correlation length and the angular directions are again important, the absolute magnitude of α is nearly linearly proportional to the magnetic field pressure (e.g. Balbus & Hawley 1991). Furthermore, the effective value of α should be obtained by averaging over the whole hot flow, whereas for ϕ only the intermediate layers are important.

For these reasons there is a broad spectrum of theoretical possibilities in the magnitude of the ratio ϕ/α . For a small correlation length and near equipartition fields, one expects $\phi \ll \alpha$, whereas for weaker fields and a larger correlation length the reverse should be true, $\phi \gg \alpha$.

One-temperature assumption We assumed here that the electron and proton temperatures are equal. This is clearly so at the cold disk and the transition layer. For the hot corona, the Coulomb interactions may be inefficient in keeping the two temperatures equal. However, even under the assumption that almost all the heating goes into protons, and only the Coulomb interactions operate, the two temperatures in a NRAF are approximately equal at radii $R \gtrsim 10^3 R_S$ (e.g. see Fig. 5 in Narayan 2002). Thus in the most “interesting” for us range of radii the one-temperature assumption should be quite reasonable.

In the innermost regions of the flow the protons may be much hotter than the electrons. Clearly the heat flux is then dominated by the protons. However, this heat flux should be of order $\phi \rho c_s^3$, i.e. only slightly lower. Hence our main argument remains the same: saturated thermal conduction will induce condensation of the hot flow when the viscous heating is weak. The physics of cooling in the transition layer will however be different for small radii (e.g. Spruit & Haardt 2000).

REFERENCES

- Abramowicz, M.A., Chen, X., Kato, S., Lasota, J.-P., & Regev, O. 1995, ApJL, 438, L37
 Albritton, J.R., Williams, E.A., Bernstein, I.B., & Swartz, K.P. 1986, PhRvL, 57, 1887
 Baganoff, F.K., Maeda, Y., Morris, M. et al. 2003, ApJ, 591, 891
 Balbus, S.A. 1986, ApJ, 304, 787
 Balbus, S.A., & Hawley, J.F. 1991, ApJ, 376, 214
 Blandford, R., & Begelman, M.C. 1999, MNRAS, 303, L1
 Cannizzo, J.K. 1998, in “Wild Stars in the Old West”, Eds. S. Howell, E. Kuulkers, & C. Woodward (San Francisco: ASP), p. 308
 Cowie, L.L., & McKee, C.F. 1977, ApJ, 211, 135
 Dewangan, G.C., Griffiths, R.E., Di Matteo, T., & Schurch, N.J. 2004, to appear in ApJ (astro-ph/0402327).
 Ditmire, T., Gumbrell, E.T., Smith, R.A., Djaoui, A., & Hutchinson, M.H.R. 1998, PhRvL. 80, 720
 Dullemond, K. 1999, A&A, 341, 936
 Elvis, M., et al. 1994, ApJS, 95, 1
 Eppelrein, E.M., & Short, R.W. 1991, Phys. Fluids B 3(11), 3092
 Esin, A. 1997, ApJ, 482, 400
 Frank, J., King, A., & Raine, D. 1992, Accretion Power in Astrophysics (Cambridge, UK: Cambridge University Press)
 Ghez, A., et al. 2003, ApJL, 586, 127
 Gierlinski, M. et al. 1999, MNRAS, 309, 496
 Ho, L.C. 1999, ApJ, 516, 672
 Ho, L.C., 2003, Active Galactic Nuclei: from Central Engine to Host Galaxy, ed. S. Collin, F. Combes, & I. Shlosman (San Francisco: ASP)
 Di Matteo, T., Allen, S.W., Fabian, A.C., Wilson, A.S., & Young, A.J. 2003, ApJ, 582, 133
 Field, G.B. 1965, ApJ, 142, 531
 Kolykhalov, P.I., & Sunyaev, R.A. 1980, Sov. Astron. Lett., 6, 357
 Krolik, J.H., McKee, C.F., & Tarter, C.B. 1981, ApJ, 249, 422
 Lasota, J.-P. 2001, New Astronomy Reviews, 45, 449
 Liu, B.F., Meyer, F., & Meyer-Hofmeister, E. 1997, A&A, 328, 247
 Luciani, J.F., Mora, P., & Virmont, J. 1983, PhRvL 51, 18
 Luciani, J.F., Mora, P., & Pellat, R. 1985, Phys. Fluids 28(3), 835
 McClintock, J.E., Narayan, R., et al. 2003, to appear in ApJ (astro-ph/0304535)
 McKee, C.F., & Cowie, L.L. 1977, ApJ, 215, 213
 McKee, C.F., & Begelman, M.C. 1990, ApJ, 358, 392
 Meyer, F., & Meyer-Hofmeister, E. 1994, A&A, 288, 175 (MMH94)
 Meyer-Hofmeister, E., & Meyer, F. 2001, A&A, 380, 739
 Narayan, R., & Yi, I. 1994, ApJL, 428, L13
 Narayan, R., & Yi, I. 1995, ApJ, 452, 710
 Narayan R. 2002, in Lighthouses of the Universe, Gilfanov, M., Sunyaev, R., & Churazov, E. (editors), Springer
 Nayakshin, S., & Svensson, R. 2001, ApJ, 551, L67
 Nayakshin, S., Cuadra, J., & Sunyaev, R. 2004, A&A, 415, 175
 Nayakshin, S., & Sunyaev, R. 2004, in preparation.
 Parker, E.N. 1973, Interplanetary Dynamical Processes, New York, Interscience.
 Penston, M.V., & Brown, F.E. 1970, MNRAS, 150, 373
 Ptak, A., Terashima, Y., Ho, L.C., & Quataert, L. 2004, to appear in ApJ (astro-ph/0401525)
 Proga, D., & Begelman, M.C., 2003, ApJ, 582, 69
 Raymond, J.C., Cox, D.P., Smith, B.W. 1976, ApJ, 204, 290
 Różańska, A., & Czerny, B. 2000a, A&A, 360, 1170
 Różańska, A., & Czerny, B. 2000b, MNRAS, 316, 473
 Schurtz, G.P., Nicolai, Ph. D., & Busquet, M. 2000, Phys. of Plasmas, 7, 4238
 Shakura, N.I., & Sunyaev, R.A. 1973, A&A, 24, 337
 Siemiginowska, A., Czerny, B., & Kostyunin, V. 1996, ApJ, 458, 491
 Spitzer, L., & Harm, R. 1953, Phys. Rev., 89, 977
 Spitzer, L. 1962, “Physics of fully ionized gases”, New York, Interscience.
 Spruit, H.C., & Haardt, F. 2000, MNRAS, 315, 751

Wood, J., Horne, K., Berriman, G., Wade, R., O'Donoghue, D., Warner, B. 1986, MNRAS, 219, 629
Zel'dovich, Ya.B., & Pickel'ner, S.B. 1969, JETP 29, 170